Enhancement and narrowing of the Aharonov-Bohm oscillations due to built-in electric field in stacked type-II ZnTe/ZnSe quantum dots: Spectral analysis

B. Roy,[1,2,*] H. Ji,[1,2] S. Dhomkar,[1,2] F. J. Cadieu,[1,2] L. Peng,[2,3] R. Moug,[3] M. C. Tamargo,[2,3] Y. Kim,[4] D. Smirnov,[4] and I. L. Kuskovsky[1,2,†]

[1]*Department of Physics, Queens College of CUNY, Flushing, New York 11367, USA*
[2]*The Graduate Center of CUNY, New York, New York 10016, USA*
[3]*Department of Chemistry, The City College of CUNY, New York, New York 10031, USA*
[4]*National High Magnetic Field Laboratory, Tallahassee, Florida 32312, USA*

(Received 28 July 2012; revised manuscript received 18 September 2012; published 11 October 2012)

Robust and narrow Aharonov-Bohm (AB) oscillations were observed in magneto-photoluminescence intensity of stacked ZnTe/ZnSe quantum dots (QDs) due to the presence of built-in electric field. A spectral analysis of such AB oscillations allowed for qualitative probing of lateral size of type-II excitons. Two samples grown using different growth sequences were analyzed and compared. The magnetic field value at which the AB transition takes place changed across the spectra for one of the samples, indicating a presence of two distinct QD stacks; a "double peak" in the AB oscillation is clearly distinguished in the spectral region where emissions from each stack overlap. The presence of built-in electric field was confirmed by behavior of the PL intensity as a function of temperature.

DOI: 10.1103/PhysRevB.86.165310 PACS number(s): 03.65.Ta, 71.35.Ji, 78.55.Et, 78.67.Hc

I. INTRODUCTION

The Aharonov-Bohm (AB) effect[1] has made significant impact on the development of physics[2,3] since its discovery in 1959. The AB effect can be typically viewed as the interference of a quantum charged particle moving along a closed trajectory in a region enclosing magnetic flux and where no classical Lorentz forces are present, thereby acquiring a quantum topological phase proportional to the enclosed magnetic flux. It was later shown that such a nontrivial quantum phase can be acquired by a moving electric dipole in a magnetic field.[4–6]

It was predicted that the AB effect for the dipole can be observed via optical emission of radially polarized excitons in nanorings and disk-like type-II quantum dots (QDs)—so-called excitonic AB effect—due to the interaction of the dipole associated with the polarized excitons with the vector potential.[7,8] The experimental verification of the AB signature of such spatially indirect excitons[9–12] inspired further interest in both theoretical[13–19] and experimental[20–26] research.

Recently, the excitonic AB effect has earned greater scientific significance because of the possibility of AB exciton storage in nanoscale quantum rings (QR) via application of an in-plane electric field,[13] an experimental observation of effects of the built-in electric field on AB interference,[21] as well as tunability and enhancement of AB effect due to the electric field.[15,23] These effects hold the possibility of realizing quantum information applications via manipulation of light and excitons with externally applied magnetic and electric fields.

Optical manifestation of the AB effect is usually observed in terms of the oscillation in excitonic energy,[9,10,24] which are very small in energy scale, and difficult to resolve,[10,12,21] and/or photoluminescence (PL) intensity.[11,22,24,25] Regarding the latter, oscillations in the integrated intensity have been commonly demonstrated, which can be explained as an averaged emission from all emission centers contributing to the PL spectra. Although excitons in type-II QDs are particularly sensitive to the AB effect due to relatively larger spatial separation of the charged particles, more reports are available for QR systems,[9,13,14,18,20,21] than for type-II QDs of suitable geometry.[10,11,17,25]

In this work, we report narrow (in magnetic field) and robust AB oscillations in the intensity of magneto-PL from stacked type-II ZnTe/ZnSe QDs. Such enhancement and narrowing of AB oscillations is due to the presence of built-in electric field. A detailed spectral analysis of the AB oscillations allows us to infer contributions from different emission centers. For example, the lateral excitonic radius is determined with subnanometer precisions using the knowledge of variation in the AB transition magnetic field, B_{AB}, as a function of energy of emitted photons.[27] We present results of such an analysis for the B_{AB} as well as the magnitudes of the AB oscillations from differently grown samples; we use these dependencies to discern the role of tellurium in formation of QDs and determine the spatial distribution of excitonic wavefunctions.

II. EXPERIMENTAL

The structures studied here are stacked type-II ZnTe/ZnSe QDs grown via migration-enhanced epitaxy using one (sample A) or three (sample B) submonolayer deposition cycles of Zn-Te-Zn sandwiched between nominally undoped ZnSe barriers. Figure 1 shows a schematic of the stacked system with applied magnetic field in the Faraday geometry and the in-plane component of built-in electric field. The growth procedure and the results of optical characterization of similar samples were reported in Refs. 28–30, and references therein.

PL measurements (at zero magnetic fields) were done with a TriVista SP2 500i Triple monochromator coupled with a thermoelectrically cooled CCD camera. The optical excitation was achieved with the 351-nm line of an Ar-ion laser. The magneto-PL experiments were performed in the Faraday geometry either with a 14 T (NHMFL) or with a 9 T (Queens College of CUNY) superconducting magnet outfitted with fiber optic probes, used to excite and collect the PL. Here, the PL was excited by a 405-nm diode laser. The detection of

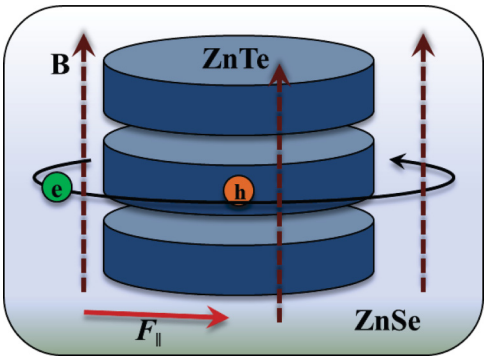

FIG. 1. (Color online) Schematic of the stacking of QDs; type-II exciton is comprised by the electron in ZnSe and the hole strongly confined within the ZnTe QD. The magnetic field (**B**) is applied in the Faraday geometry. Such a configuration is ideal for observation of AB effect. $\boldsymbol{F}_{\parallel}$ indicates the in-plane component of the built-in electric field in the system.

magneto-PL experiments was done by a portable Ocean Optics solid-state spectrometer.

III. RESULTS AND DISCUSSIONS

A. Photoluminescence

Low temperature (∼10 K) PL spectra are shown in Fig. 2. The PL signal from sample A consists of a broad blue band overlaid with sharp lines (at ∼2.66, 2.695, 2.726, 2.757, and 2.767 eV) along with small peaks at ∼2.693, 2.717, 2.748, and 2.765 eV [Fig. 2(a)].[31] The first two sharp lines (2.767 and 2.757 eV) are zero phonon lines; one can resolve at least three phonon replicas at 2.726, 2.695, and 2.66 eV (ZnSe LO phonon energy is ∼31 meV). Apart from the distinctive sharp lines generally seen in samples grown with minimal Te concentration, this sample shows the signature of coexistence of $Te_{(n\geqslant 2)}$ isoelectronic centers (ICs) and the QDs.[31] The latter could only be observed at elevated temperatures, when the band edge PL is suppressed due to thermal ionization of isoelectronic bound excitons (IBEs). Excitation intensity-dependent PL at low temperature does not reveal significant shift in peak energy for the "blue band"-dominant transitions as shown in the inset of Fig. 2(a), the excitation intensity dependence of emission energy at 20% height of the peak on the lower energy side.

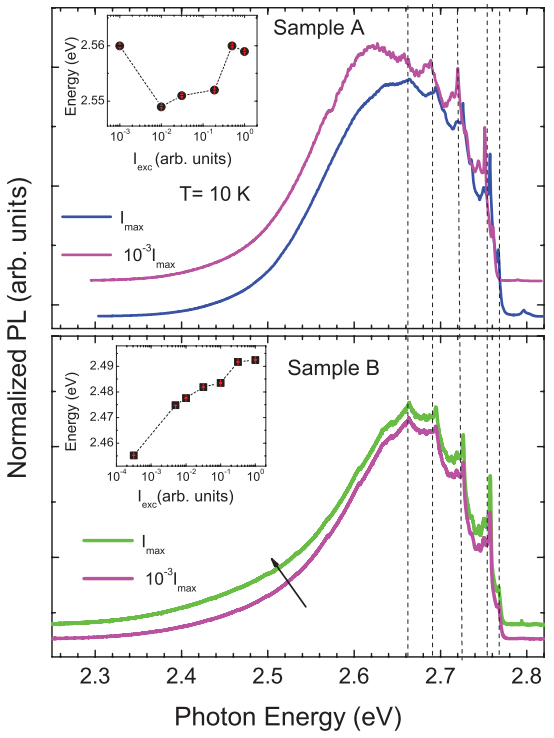

FIG. 2. (Color online) Low-temperature PL at two excitation intensities for (a) sample A and (b) sample B. Dashed lines are for eye guidance only. Inset shows the excitation intensity dependence of emission energy at 20% height of the peak on the lower-energy side.

In sample B, grown with three Zn-Te-Zn deposition cycles, the QDs dominated PL (generally seen as a broad "green band" with peak around 2.5 eV, and sometimes with a low energy shoulder,[12] and as low as 2.3 eV[30,32]) is convoluted with the emission due to IBEs.[28] This triple-cycle sample exhibits a high degree of separation of QD containing layers from the barriers as observed by the presence of the band edge emission, which previously was seen *only* in samples grown with a single Zn-Te-Zn MEE cycle (e.g., as seen in sample A).[31] We note that the sharp lines are seen at same energies (∼2.66, 2.694, 2.726, 2.757, and 2.767 eV) as for sample A. The excitation intensity-dependent PL, however, shows blue shift of ∼37 meV in emission energy at the "green band" energy position. In Fig. 2(b), two different excitation intensity PL plots are overlaid for eye guidance.

B. Magnetophotoluminescence: Integrated intensity

Due to the cylindrical symmetry, the exciton ground state in stacked type-II disk-like QDs initially has a zero orbital angular momentum, which changes to higher values with increasing magnetic field. This transition of the angular momentum to a nonzero value influences the optical properties as:[8] the ground-state energy oscillates as the orbital angular-momentum states cross and the PL intensity changes due to optical selection rules. Experimentally, the latter is often observed as one or more oscillations ("peaks"), which can arise due to such factors as QD shape anisotropy, e.g., elongation,[9] presence of impurities,[19,21] and/or built-in electric field.[15] In such cases, the excitonic states do not possess a definite value of the angular momentum and optical selection rules are relaxed. Also, in real experimental conditions, where the whole system is in the magnetic field, the wavefunction of one carrier is "squeezed" closer and "pushed" away to the QD boundary before and after the angular momentum transition, respectively, which leads to an increase followed by a decrease in the PL emission. In the case that one of the carriers is strongly confined in the QDs, as the hole in our material system,[11,12] the lowest exciton state as a function of the magnetic field will undergo the transition to nonzero orbital momentum at such a magnetic field, B_{AB}, that

$$\pi R_e^2 B_{\mathrm{AB}} = \Phi_0/2, \tag{1}$$

where $\Phi_0 = h/e$ is the flux quantum, R_e is the radius of the electronic orbit, and h and e are the Planck's constant and the electron charge, respectively.

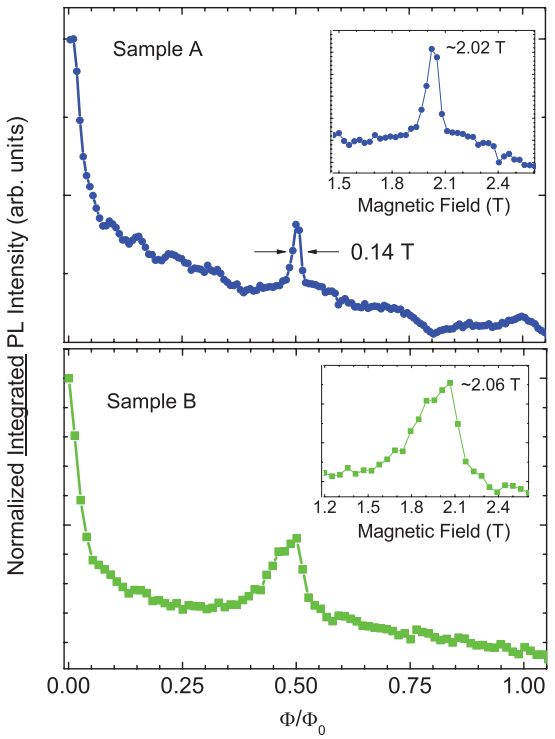

FIG. 3. (Color online) Normalized integrated PL intensity as a function of normalized magnetic flux for (a) sample A and (b) sample B. Insets show enlarged peak region as a fucntion of the magnetic field.

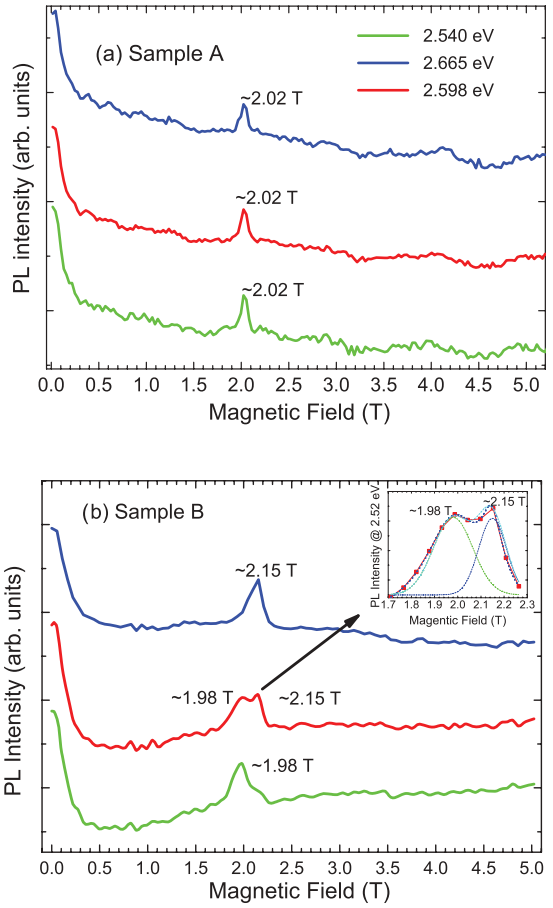

FIG. 4. (Color online) Magneto-PL at three spectral position of spectrum of Fig. 1, showing the AB oscillations of (a) sample A and (b) sample B. Inset in (b) shows enlarged picture of "double AB peak" as seen in sample B at 2.52 eV.

In Figs. 3(a) and 3(b), we show the normalized integrated PL intensity as a function of the normalized magnetic flux for samples A and B, respectively. The insets of Figs. 3(a) and 3(b) show the peak at B_{AB} values ∼2.02, 2.06 T for each sample. Using Eq. (1), the characteristic radius of electronic orbit was determined to be 18.0 and 17.8 nm for samples A and B, respectively. Considering that the stacking of QDs results in averaging out size variations in QDs and that at low temperature the $L = 0$ (i.e., ground state) dominates, the magnetic flux was calculated for corresponding area enclosed by the electron trajectory with the goal to compare our observations with theoretical calculations for QRs.[13] The oscillation is at $\Phi/\Phi_0 = 1/2$. The magnitude of the AB oscillation relative to the background in integrated PL is 3 to 4% for these samples. We show below that the magnitude of the oscillations is even larger for specific emission energies, and it reaches 6% for sample A and 4% for sample B. The full-width-at-half-maximum (FWHM) of the oscillation in the normalized magnetic flux is ∼0.02 for sample A and ∼0.06 for sample B. Such magnitude of the AB oscillation peak is larger[22,25] and the peaks are significantly narrower[21,22,25] than the values reported in the literature for both QDs[22,25] and QRs.[13,21]

We compare the widths of the AB "peaks" with theoretical predictions available for type-I QRs[13] even though there is a critical difference between the two systems, since we are not aware of such calculations for type-II QDs. Without the electric field, the FWHM of ∼0.3 in units of normalized magnetic flux has been predicted for the bright excitons. This is substantially wider than what we observe for both samples; however, if one assumes presence of a strong in-plane electric field ($u_0 = 0.3$ in Ref. 13 notations) then the observed FWHM can easily be explained and understood. Moreover, the electric field also leads to enhancement of the AB effect,[15,20,21] explaining such robust oscillation. For instance, in the presence of the built-in electric field, a relatively large (∼9%) AB oscillation in intensity was seen for some of the QRs described in Ref. 21.

The built-in electric field in a zinc-blende system grown along [001], like ours, can have piezo-electric origin due to anisotropic strain.[33,34] In epitaxially grown ZnTe/ZnSe system, during the QD growth, the strain fields arise due to the lattice mismatch between the ZnTe QDs and ZnSe matrix;[35] the anisotropic nature of the strain is supported by the following observations:

(i) as reported previously, some QDs in these systems are elongated,[11] which can lead to anisotropic strain, similar to that reported for InGaAs/GaAs QR;[21]

(ii) the vertical correlation, required to form stacks, strongly indicates the presence of elastic anisotropy that plays crucial role for effective lateral and/or vertical self-organization in QD superlattices;[36] vertical correlation of stacked QDs in a similar system of type-II ZnMgTe/ZnSe superlattice was reported recently.[37]

We hope to stimulate the theoretical investigations of the magnetic field-dependent oscillator strength with and without

the presence of an electric field, for type-II QDs specifically, in order to confirm our hypothesis. We also report in later section an experimental signature of presence of built-in electric field in our sample.

C. Magnetophotoluminescence: Spectral analysis

To get insight into the material structure of the samples, we performed a more detailed investigation by tracking the AB oscillations at various energies across the PL spectrum for each sample. In Figs. 4(a) and 4(b), we show for samples A and B, respectively, the AB oscillation in PL intensity at three different spectral energies, corresponding to the lower- and higher-energy sides as well as the peak of the spectrum. We derive interesting observations; e.g., for sample A, the AB peak is seen at a constant B_{AB} value of ∼2.02 T for all three energies (2.540, 2.598, and 2.664 eV), whereas for sample B, the AB oscillation shows a distinctive change in values of B_{AB}. Moreover, careful examination of the transition region displays a "double AB peak," as plotted for 2.52 eV, for sample B [inset of Fig. 4(b)].

As seen from Eq. (1), the B_{AB} value is determined by the radius of the electronic orbit. So we infer for sample B that the electronic orbit changes across the PL spectra, which signifies the presence of more than one stack of QDs with different effective radii for the orbiting electron. This allowed us to determine the size of the type-II exciton with subnanometer precisions.[27] However, in sample A, B_{AB} does not change significantly, so the radius of electronic orbit is the same across the spectrum; we conclude from such an observation that only one QD stack is present in sample A. We also note that the FWHM of each of the AB peaks [∼0.12 to 0.17 T, shown in inset of Fig. 4(b)] comprising the "double peak" in sample B is comparable to the FWHM of the AB peak in sample A (∼0.14 T), suggesting that two QD stacks in sample B have similar properties to the QDs of sample A. This also suggests that both samples have a similar built-in electric field, which originates in the lattice mismatch between ZnTe and ZnSe.

To strengthen these conclusions and to obtain a more complete picture, we show in Figs. 5 and 6 the behavior of B_{AB} and the magnitude of AB oscillations as a function of the PL spectral energy for both samples. Figures 5(a)–5(c) show the spectral analysis of low-temperature magneto-PL in sample A. The spectral behavior of B_{AB} and the magnitude of oscillation are plotted in Figs. 5(b) and 5(c), respectively, which are related to the PL shown in Fig 5(a). The magnitude is determined with regard to the background emission intensity.

No significant change in B_{AB} across the spectral positions was observed for sample A, which indicates almost no distinguishable excitonic size variation. The PL spectrum is decomposed into two Gaussian peaks [Fig. 5(a)] attributed to the presence of "green" (∼2.56 eV) and a cumulative "blue" (∼2.68 eV) band, which can be associated to the QD- and IC-dominated emissions, respectively.

We show the spectral plots of B_{AB} and the magnitude of oscillation for sample B in Figs. 6(a)–6(c). We observe B_{AB} changes from a lower value of ∼1.98 T at the lower-energy side (below ∼2.47 eV) to a higher value of ∼2.15 T at the higher-energy side (above ∼2.55 eV) for sample B. The error in determination of B_{AB} is less than the observed change (also

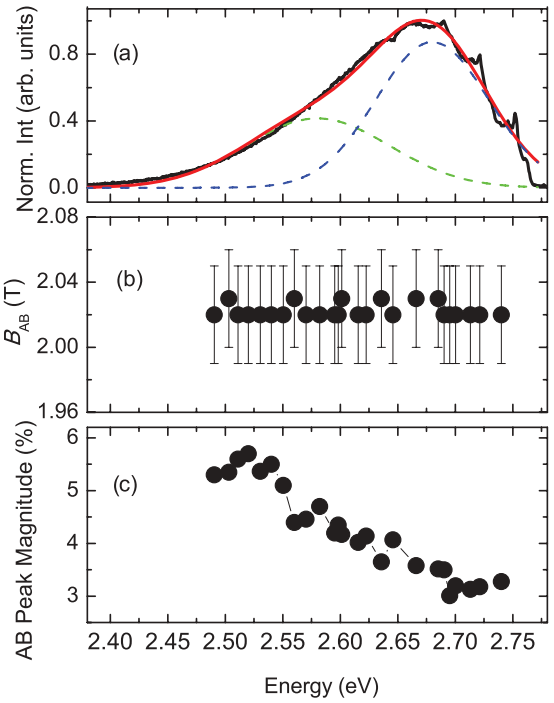

FIG. 5. (Color online) Spectral analysis of AB oscillations in sample A: (a) PL spectrum decomposed into two Gaussians; (b) B_{AB}; (c) Magnitude of the AB oscillations.

displayed in the plot). An average of the B_{AB} is represented from the two peaks as observed in the "double AB peak" [Fig. 6(b)] to indicate the transition in B_{AB}. The "double peak" B_{AB} values are also shown in Fig. 6(b) (blue and green markers)

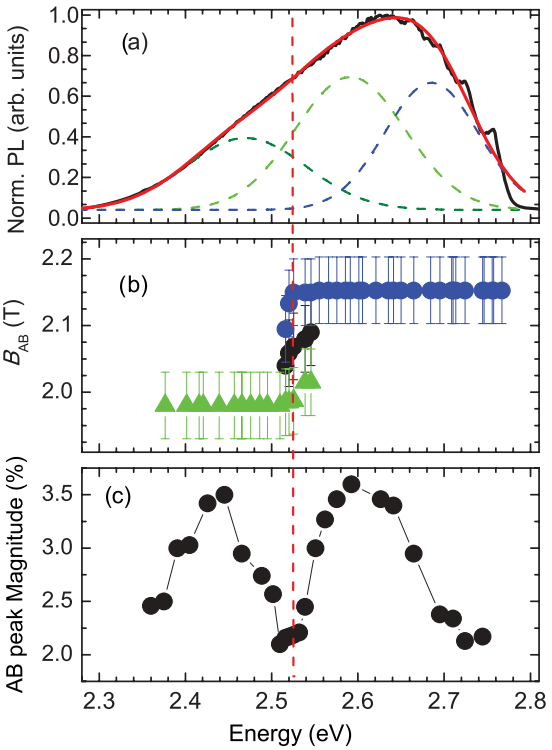

FIG. 6. (Color online) Spectral analysis of AB oscillation in sample B: (a) PL spectrum decomposed into three Gaussians; (b) B_{AB}; (c) magnitude of the AB oscillations.

for the transition spectral region. The transition of B_{AB} from a lower value to a higher one is observed within a relatively narrow spectral range—between 2.49 and 2.54 eV.

To relate such an observation to the PL spectra, three Gaussian peaks were used to decompose the PL [Fig. 6(a)]; the "green" band is formed by two Gaussians ("Green band 1" at ∼2.59 eV and "green band 2" at ∼2.48 eV) with comparable weights, while the third Gaussian represents a "combined blue" band for the higher energies dominated by the IBEs. Under such conditions, the best fitting resulted in a "reduced" overlap of the lower energy Gaussians in the close proximity of the spectral region of interest, indicating that the change in transition field is observable due to the subdued emission from the two overlapping PL bands. The contribution from two different type-II excitons also explains the asymmetry of the AB peak in the integrated intensity, as the emission of one of the excitons dominate in a specific spectral region.

The difference in the PL peak energy between these two stacks, estimated from the peaks of the two Gaussians used to form the green band, is ∼110 meV. Such a large difference is unattainable by any realistic change in the QD radius;[38] thus, other factors, such as thickness, chemical composition of QDs, and strain, which can change the band offsets (which determine the potential seen by the electron), are also significant in understanding of the observed PL. Thus, we suggest that the two stacks are distinguishable not only in terms of radius of electronic orbit or the lateral sizes of QDs, but also due to the change in QD thickness and/or change in the band offsets because of the variations in Te composition.

D. Magnitude of the Aharonov-Bohm oscillations

The spectral variation of the magnitude of the AB peak is shown in Figs. 5(c) and 6(c). The magnitude of an AB oscillation is expected to be related to the change in the oscillator strength of the exciton during the AB transition. The change in the oscillator strength is predicted to be smaller with a larger oscillator strength (or the overlap integral between electron and hole wavefunctions) in QRs, due to favorable AB configuration,[15] whereas no such theoretical predictions for type-II QDs are available, to the best of our knowledge. Our observations, however, contradict this conclusion at least partially, as it would then be expected for "smaller" dots, the stronger oscillator strength[15,39] would give rise to a smaller AB amplitude. In sample A, we do observe such a trend in the magnitude of oscillation, even though we did not see any change in B_{AB} (which suggests almost constant size of the QD stacks). For sample B, we observe a variation in the magnitude of the AB oscillation for both lower- and higher-energy sides of the spectra with a decrease in the AB amplitude at the transition spectral region. The maximum magnitude for each stack is almost the same, although the corresponding excitons have different sizes, and therefore different overlap integrals. We intend to address this aspect in greater detail in future work.

E. Temperature dependence and confirmation of built-in electric field

We also investigated the temperature dependence of PL to verify the presence of built-in electric field. In Fig. 7, the behavior of integrated intensity of each of the three contributing bands from the PL of sample B [as decomposed in Fig. 6(a)] is shown as a function of temperature. The decrease of the PL intensity with increasing temperature is expected, due to the increase in nonradiative transitions and luminescence quenching. However, we also observed an initial increase of the PL intensity with temperature for $T < 80$ K, which is eminent at the QD-dominated lower-energy green band (∼2.48 eV). This is a signature of the presence of built-in electric field, which has been theoretically investigated via calculation of oscillator strength in the presence of electric field and also experimentally observed for InAs/GaAs QRs.[21] It was suggested that with electric field, the oscillator strength can increase by the activation of more efficient channels for optical recombination at excited states with electron-hole separation smaller than in the ground state. We clearly observe a similar behavior which confirm the presence of built-in electric field in these stacked type-II ZnTe/ZnSe QDs.

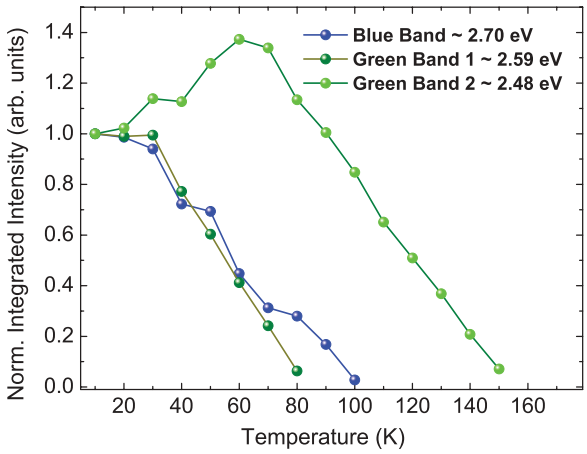

FIG. 7. (Color online) The temperature dependence of integrated PL intensity for sample B showing signature of built-in electric field in the sample.

IV. SUMMARY

In summary, we investigated AB oscillations in stacked ZnTe/ZnSe QDs in the presence of built-in electric field that causes robust and narrow oscillations, which was previously studied only in QR systems. Such robust AB effect can be exploited toward achieving novel applications related to exciton storage and retrieval by control of external fields. We also developed a spectral analysis approach to probe the lateral distribution of QDs in these systems. High-precision estimation of radius of the type-II excitonic lateral size was possible. Spectral behaviors of a triple cycle deposited Zn-Te-Zn sample and a single-cycle deposited sample are discussed and presence of two distinguishable QD stacks for the former and only one set of QD stacks for the latter is revealed. Appearance of "double AB peak" in intensity at spectral regions with finite overlap of the two decomposed green bands clearly indicates transition of dominance from one set of QDs stack to another within the transition spectral region. The temperature dependence of the decomposed bands confirmed the presence of built-in electric field, which was previously reported for QRs. The behavior of magnitude of

oscillation is not completely understood and we intend to address this issue in upcoming work.

ACKNOWLEDGMENTS

This work is supported by the National Science Foundation under Award No. 40A94-0001. The samples used in this study are grown under Department of Energy, Basic Energy Sciences Grant No. DE-FG02-10ER46678. A portion of this work was performed at the NHMFL, which is supported by NSF Cooperation Agreement No. DMR-0084173 and by the State of Florida. The authors are thankful to D. Sarkar, U. Manna, A. Lisyansky, L. Mourokh, and I. C. Noyan for helpful discussions and support.

*bidisha@physics.qc.edu
†igor.kuskovsky@qc.cuny.edu

[1] Y. Aharonov and D. Bohm, Phys. Rev. **115**, 485 (1959).
[2] S. Popescu, Nat. Phys. **6**, 151 (2010).
[3] H. Batelaan and A. Tonomura, Phys. Today **62**, 38 (2009).
[4] M. Wilkens, Phys. Rev. Lett. **72**, 5 (1994).
[5] H. Wei, R. Han, and X. Wei, Phys. Rev. Lett. **75**, 2071 (1995).
[6] G. Spavieri, Phys. Rev. Lett. **82**, 3932 (1999).
[7] A. B. Kalametsev, V. M. Kovalev, and A. O. Govorov, JETP Lett. **68**, 669 (1998).
[8] A. O. Govorov, S. E. Ulloa, K. Karrai, and R. J. Warburton, Phys. Rev. B **66**, 081309(R) (2002).
[9] M. Bayer, M. Korkusinski, P. Hawrylak, T. Gutbrod, M. Michel, and A. Forchel, Phys. Rev. Lett. **90**, 186801 (2003).
[10] E. Ribeiro, A. O. Govorov, W. Carvalho, Jr., and G. Medeiros-Ribeiro, Phys. Rev. Lett. **92**, 126402 (2004).
[11] I. L. Kuskovsky, W. MacDonald, A. O. Govorov, L. Muroukh, X. Wei, M. C. Tamargo, M. Tadic, and F. M. Peeters, Phys. Rev. B **76**, 035342 (2007).
[12] I. R. Sellers, V. R. Whiteside, I. L. Kuskovsky, A. O. Govorov, and B. D. McCombe, Phys. Rev. Lett. **100**, 136405 (2008).
[13] A. M. Fischer, V. L. Campo, Jr., M. E. Portnoi, and R. A. Römer, Phys. Rev. Lett. **102**, 096405 (2009).
[14] F. Palmero, J. Dorignac, J. C. Eilbeck, and R. A. Römer, Phys. Rev. B **72**, 075343 (2005).
[15] B. Li and F. M. Peeters, Phys. Rev. B **83**, 115448 (2011).
[16] L. G. G. V. Dias da Silva, S. E. Ulloa, and A. O. Govorov, Phys. Rev. B **70**, 155318 (2004).
[17] K. L. Janssens, B. Partoens, and F. M. Peeters, Phys. Rev. B **64**, 155324 (2001).
[18] V. M. Fomin, V. N. Gladilin, S. N. Klimin, J. T. Devreese, N. A. J. M. Kleemans, and P. M. Koenraad, Phys. Rev. B **76**, 235320 (2007).
[19] H. Hu, J.-L. Zhu, D.-J. Li, and J.-J. Xiong, Phys. Rev. B **63**, 195307 (2001).
[20] A. V. Maslov and D. S. Citrin, Phys. Rev. B **67**, 121304 (2003).
[21] M. D. Teodoro, V. L. Campo, Jr., V. Lopez-Richard, E. Marega, Jr., G. E. Marques, Y. G. Gobato, F. Iikawa, M. J. S. P. Brasil, Z. Y. AbuWaar, V. G. Dorogan, Yu. I. Mazur, M. Benamara, and G. J. Salamo, Phys. Rev. Lett. **104**, 086401 (2010).
[22] I. R. Sellers, V. R. Whiteside, A. O. Govorov, W. C. Fan, W. C. Chou, I. Khan, A. Petrou, and B. D. McCombe, Phys. Rev. B **77**, 241302 (2008).
[23] F. Ding, N. Akopian, B. Li, U. Perinetti, A. Govorov, F. M. Peeters, C. C. Bof Bufon, C. Deneke, Y. H. Chen, A. Rastelli, O. G. Schmidt, and V. Zwiller, Phys. Rev. B **82**, 075309 (2010).
[24] S. Miyamoto, O. Moutanabbir, T. Ishikawa, M. Eto, E. E. Haller, K. Sawano, Y. Shiraki, and K. M. Itoh, Phys. Rev. B **82**, 073306 (2010).
[25] M. H. Degani, M. Z. Maialle, G. Medeiros-Ribeiro, and E. Ribeiro, Phys. Rev. B **78**, 075322 (2008).
[26] L. Schweidenback, T. Ali, A. H. Russ, J. R. Murphy, A. N. Cartwright, A. Petrou, C. H. Li, M. K. Yakes, G. Kioseoglou, B. T. Jonker, and A. Govorov, Phys. Rev. B **85**, 245310 (2012).
[27] B. Roy, H. Ji, S. Dhomkar, F. J. Cadieu, L. Peng, R. Moug, M. C. Tamargo, and I. L. Kuskovsky, Appl. Phys. Lett. **100**, 213114 (2012).
[28] Y. Gu, I. L. Kuskovsky, M. van der Voort, G. F. Neumark, X. Zhou, and M. C. Tamargo, Phys. Rev. B **71**, 045340 (2005).
[29] I. L. Kuskovsky, Y. Gu, M. van der Voort, C. Tian, B. Kim, I. P. Herman, G. F. Neumark, S. P. Guo, O. Maksimov, and M. C. Tamargo, Phys. Status Solidi B **229**, 239 (2002).
[30] B. Roy, A. Shen, M. Tamargo, and I. Kuskovsky, J. Electron. Mater. **40**, 1775 (2011).
[31] I. L. Kuskovsky, Y. Gong, G. F. Neumark, and M. C. Tamargo, Superlattices Microstruct. **47**, 87 (2010).
[32] M. C. K. Cheung, A. N. Cartwright, I. R. Sellers, B. D. McCombe, and I. L. Kuskovsky, Appl. Phys. Lett. **92**, 032106 (2008).
[33] A. G. Kontos, N. Chrysanthakopoulos, M. Calamiotou, T. Kehagias, P. Komninou, and U. W. Pohl, J. Appl. Phys. **90**, 3301 (2001).
[34] K. Hingerl, R. E. Balderas-Navarro, A. Bonanni, and D. Stifter, J. Vac. Sci. Technol. B **19**, 1650 (2001).
[35] S. J. Kim, B.-C. Juang, W. Wang, J. R. Jokisaari, C.-Y. chen, J. D. Phillips, and X. Q. Pan, J. Appl. Phys. **111**, 093524 (2012).
[36] V. Holý, G. Springholz, M. Pinczolits, and G. Bauer, Phys. Rev. Lett. **83**, 356 (1999).
[37] U. Manna, I. C. Noyan, Q. Zhang, I. F. Salakhutdinov, K. A. Dunn, S. W. Novak, R. Moug, M. C. Tamargo, G. F. Neumark, and I. L. Kuskovsky, J. Appl. Phys. **111**, 033516 (2012).
[38] Note: We calculated the hole confinement energy inside a cylindrical dot of radius a and thickness d; The energy is given by $E = \frac{\hbar^2}{2m_h^*}[x_{ms}^2 + \frac{n_z^2\pi^2}{d^2}]$ where m_h^* is the effective mass of hole in ZnTe, x_{ms} are the solutions for $\frac{J_1(x_{ms})}{J_0(x_{ms})} = \frac{N_1(x_{ms})}{N_0(x_{ms})}$; where $J(x_{ms})$ and $N(x_{ms})$ are the Bessel functions of the first and the second kind, respectively, taken for $m = 0$ and $s = 1$. For ground state: $n_z = 1$ and with realistic values of dot radii ~9 to 11 nm, $d = 1$ nm, the energy is observed to change by ~0.1 to 0.2 meV.
[39] J. M. Rorison, Phys. Rev. B **48**, 4643 (1993).